Phys Chem Minerals (2004) 31: 465–474
DOI 10.1007/s00269-004-0413-z

ORIGINAL PAPER

G. D. Gatta · S. A. Wells

Rigid unit modes at high pressure: an explorative study of a fibrous zeolite-like framework with EDI topology

Received: 1 April 2004/Accepted: 5 June 2004

Abstract We report a comparative study on the high pressure (H*P*) structural behaviour of a fibrous zeolite (with EDI topology) on the basis of rigid unit modes (RUM) modelling and previously published single-crystal X-ray diffraction. H*P* single-crystal diffraction data lead to a more precise determination of the elastic parameters (axial and volume compressibilities) useful to define the equation-of-state under isothermal conditions, and the structural refinements are useful to describe the main deformation mechanisms of the Si/Al framework and extra-framework content at high pressure. The RUM modelling is applied to simulate the compressive behaviour of the framework, under hydrostatic and non-hydrostatic conditions, using a minimum number of parameters, and to describe the deformation mechanism intuitively in terms of the rotations of the SiO_4 polyhedra. The local and global *P*-induced deformation mechanisms of the Si/Al framework observed in experiment (channel ellipticity, SBU rotation) are well reproduced by RUM modelling. The simulation of uniaxial compression (non-hydrostatic conditions) shows an interesting result on the structural behaviour. This comparative study tests the reliability of the RUM modelling in open-framework silicates with a complicated crystal structure.
Electronic Supplementary Material. Supplementary material to this paper is available in electronic form at http://dx.doi.org/10.1007/s00269-004-0413-z.

G. D. Gatta (✉)
Bayerisches Geoinstitut,
Universitaet Bayreuth,
Universitaet Str. 30,
95447 Bayreuth, Germany
e-mail: diego.gatta@uni-bayreuth.de
Tel.: +49 (0)921 55 3745
Fax: +49 (0)921 55 3769

S. A. Wells
Davy Faraday Research Laboratory,
21 Albemarle Street
London W1 S 4BS, UK

Keywords Fibrous zeolite · Edingtonite · High pressure single-crystal X-ray diffraction · Rigid unit modes

Introduction

Natural and synthetic microporous and mesoporous framework silicates are receiving increasing attention due to their technological applications in several industrial fields (Kallo 2001; Tchernev 2001; Ming and Allen 2001; Bish et al. 2003; Zheng et al. 2003). For this reason, the thermal and catalytic properties of these materials have been investigated extensively. On the other hand, only a few studies have been dedicated to the high pressure behaviour of open-framework silicates. As noted by Gatta et al. (2003), the presence of open cavities (cages) and channels makes these materials an interesting and suitable model for phenomena related to polyhedral tilt transitions. Furthermore, the H*P*-elastic parameters of the zeolites allow the determination of their isothermal equation-of-state (EoS). Several of the few studies on zeolites under pressure have been dedicated to the fibrous zeolite group. Belitsky et al. (1992) reported on the pressure-induced transformations in natrolite and edingtonite, which they investigated using spectroscopic (Raman, NMR) and diffraction data. The authors showed that different behaviour occurs when using penetrating and non-penetrating pressure transmitting media. An overhydration effect on the natrolite was observed using a hydrous pressure medium. An H*P*-synchrotron powder diffraction study on natrolite (Lee et al. 2002) confirmed that pressure transmitted by penetrating fluids induces a phase transition due to superhydration: a selective sorption of water expands the channels along the *a* and *b* unit-cell axes.

H*P*-induced amorphization of scolecite and mesolite, investigated using synchrotron powder diffraction data and Raman spectroscopy, was reported by Gillet et al. (1996). A comparative study on the pressure-induced structural modifications in scolecite by means of in-situ synchrotron X-ray powder diffraction and density

functional computations was performed by Ballone et al. (2002). A further paper of Comodi et al. (2002) on the H*P* behaviour of scolecite, using single-crystal diffraction data, showed the main deformation mechanisms under pressure and reported the isothermal equation-of-state of this zeolite.

A high pressure Raman study of edingtonite in a diamond-anvil cell at room temperature reported by Goryainov et al. (2003) shows that there is no pressure-induced phase transition up to 6.4 GPa. Lee et al. (2004) investigated the H*P*-behaviour of edingtonite and thomsonite by in-situ synchrotron powder diffraction using a nominally penetrating pressure medium. The authors emphasized the anisotropic compression up to 6 GPa, without evidence of phase transition within the pressure range investigated.

The aim of our study is to compare the structural evolution of tetragonal edingtonite under pressure using two different approaches: by in-situ X-ray single-crystal diffraction, using the experimental data recently published by Gatta et al. (2004), and by rigid unit modes (RUM) modelling (Dove et al. 1995; 1996; Hammonds et al. 1997; Wells et al. 2002a,b; Wells 2003). H*P* single-crystal diffraction data lead to a more precise determination of the elastic parameters (axial and volume compressibilities), which are useful to define the isothermal EoS, and the structural refinements allow us to describe the main deformation mechanisms of the framework and extra-framework content under pressure. The RUM modelling allows us to model the compressive behaviour of the framework using a minimum number of parameters, and to describe the deformation mechanism intuitively in terms of the rotations of the SiO_4 polyhedra.

This comparison is useful to test the reliability of the RUM modelling in open-framework silicates with a complicated crystal structure.

Crystal structure of edingtonite

Edingtonite is a barium fibrous zeolite (Gottardi and Galli 1985; Armbruster and Gunter 2001) and its ideal chemical composition is $Ba_2Al_4Si_6O_{20}{\cdot}8H_2O$. The crystal structure of edingtonite was first determined by Taylor and Jackson (1933) in the $P\bar{4}2_1m$ space group, though the authors did not exclude orthorhombic symmetry. Galli (1976) and Kvick and Smith (1983) refined the crystal structure in $P\ 2_12_12$ by single-crystal X-ray and neutron diffraction data, respectively. The difference between tetragonal and orthorhombic edingtonite is due to (Si,Al) order–disorder in the tetrahedra, which reduces the lattice symmetry from $P\bar{4}2_1m$ to $P\ 2_12_12$. Mazzi et al. (1984) reinvestigated the crystal structure of tetragonal edingtonite, giving new details on the topological configuration of the extra-framework content.

The Si/Al framework of this fibrous zeolite (framework type code: EDI, Baerlocher et al. 2001) consists of tetrahedral chains, with topological symmetry $P\bar{4}2_1m$, running along [001] (Fig. 1). The basic unit for these chains is the $4 = 1$ secondary building unit (SBU) (Baerlocher et al. 2001), shown in Fig. 1. The framework encloses two systems of channels: eight-ring channels along [001] and eight-ring channels along [110], in which the extra-framework cations and water molecules lie. With respect to the other fibrous zeolites, in edingtonite the SBU chains are linked without any relative translation between the chains (Gottardi and Galli 1985; Armbruster and Gunter 2001). In contrast, natrolite, scolecite,

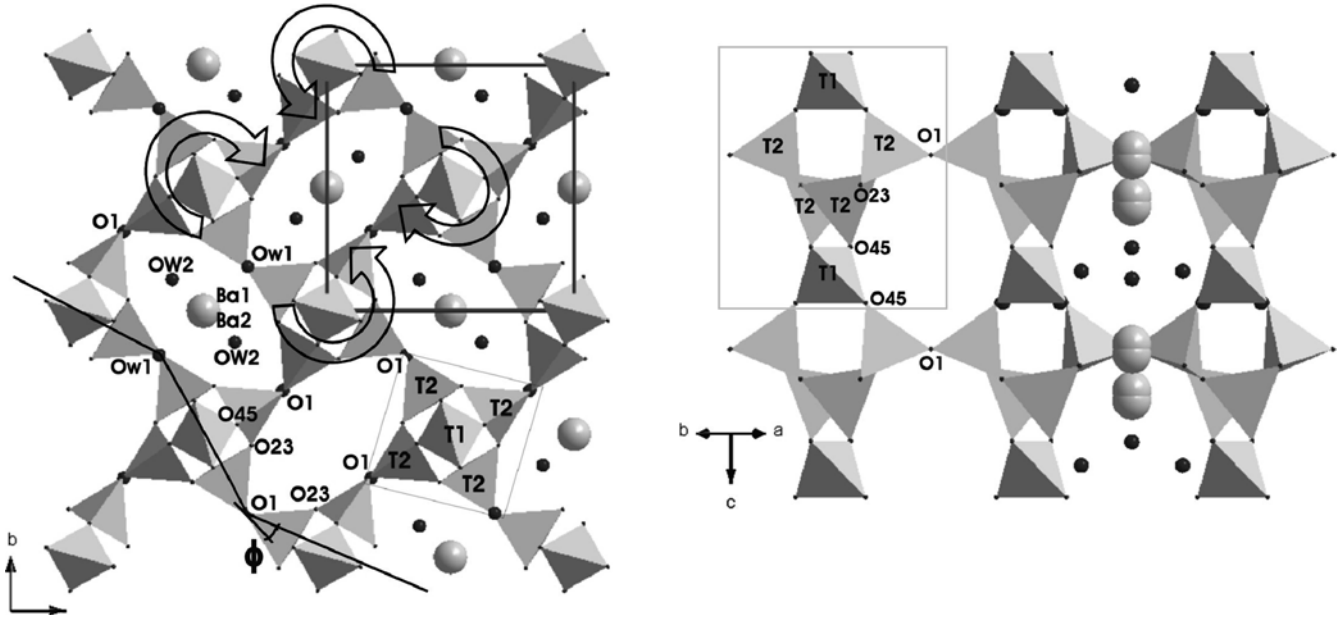

Fig. 1 Crystal structure of tetragonal edingtonite, viewed down [001] (*left*) and down [110] (*right*). The SBU is highlighted (bracketed). The pressure-induced antirotation mechanism is shown

mesolite and thomsonite show translations of about 1.65 Å along the *c*-axis. Since the shape and the free volume of the [001] channels are strongly influenced by the cross-linking of the SBU chains, the crystal structure of edingtonite is characterized by the largest channels with respect to the other fibrous zeolites. Thus, large cations (e.g. Ba, Sr, Ca) can reside in the [001]-channels. In the crystal structure of edingtonite, the extra-framework content is represented by one cation site (preferentially occupied by Ba) and by two independent water molecule sites. The large Ba-coordination polyhedron consists of six framework oxygens and four water molecules. Mazzi et al. (1984) and Gatta and Boffa Ballaran (2004) showed that in both tetragonal and orthorhombic edingtonite the Ba site is really split into two sites $\sim$0.3–0.4 Å apart. Most of the Ba cations (more than 90%) occupy the Ba1 site and a minor amount (less than 10%) occupy the Ba2 site.

The structural thermal stability of orthorhombic edingtonite was investigated by Belitsky et al. (1986) and Ståhl and Hanson (1998) at low and high temperature, respectively.

Experimental: H*P*-single-crystal X-ray diffraction

Experimental methods

A sample of natural tetragonal edingtonite from Ice River (Canada), with unit-cell content $(Ba_{1.82}Sr_{0.01}K_{0.11}Na_{0.03})(Al_{3.90}Si_{6.13})O_{20}\cdot 7.30\ H_2O$, was used in this study. A single-crystal diffraction data collection was firstly carried out under room conditions on an XCALIBUR Oxford Instruments diffractometer equipped with CCD (using graphite monochromatized Mo$K\alpha$ radiation); 10 809 reflections in the range $6 < \theta < 70°$ were collected, of which 1371 were unique, giving metrically tetragonal cell parameters $a = b = 9.5909(10)$ Å, $c = 6.5339(10)$ Å, $V = 601.02(30)$ Å^3. After Lorentz, polarization and empirical absorption corrections using the SADABS package (Sheldrick 1996), the discrepancy factor among symmetry-related reflections was $R_{int} = 0.038$. The refinement was carried out with anisotropic displacement parameters in space group $P\bar{4}2_1m$ using the SHELXL-97 program (Sheldrick 1997), starting from the atomic coordinates of Mazzi et al. (1984). Since in the high-pressure refinements hydrogen atoms cannot be observed, these were also not included in the ambient-pressure refinement, to aid comparison.

The final agreement index [$R_1(F)$] was 0.019 for 57 refined parameters and 604 unique reflections with $F_o > 4\sigma(F_o)$. The Si/Al-disorder in the tetrahedra demonstrates the effective general tetragonal symmetry of this specimen. <T1–O> and <T2–O> bond distances are 1.654 and 1.671 Å, respectively. The same crystal was used for the H*P*-experiment.

A diamond-anvil cell (DAC) (Allan et al.1996) was used for the high pressure experiments. To avoid any overhydration effect, glycerol ($CH_2OHCHOHCH_2OH$) was used as an anhydrous non-penetrating pressure-transmitting medium, since its large molecules do not penetrate the zeolite framework channels. Two independent methods were used for pressure calibration: the ruby fluorescence method (Forman et al. 1972; Mao et al. 1986) and the EoS of quartz (Angel et al. 1997).

The lattice constants of edingtonite were measured up to 5.08 GPa on a Huber SMC 9000 four-circle diffractometer (using non-monochromatized Mo$K\alpha$ radiation) with eight-position centring of 25 Bragg reflections according to the procedure proposed by King and Finger (1979) and Angel et al. (2000). Three different data collections were performed with a Nonius-CAD4 diffractometer (using graphite monochromatized Mo$K\alpha$ radiation) at 0.0001 GPa (crystal in DAC without pressure medium), 2.28(1) and 4.61(2) GPa up to $2\theta = 60°$. Integrated intensity, pressure-cell absorption and Lorentz-polarization corrections were obtained using the programs WinIntegrSTP3.4 and ABSORB5.2 (Burnham 1966; 2002, Angel 2003a, b).

The H*P* structural refinements were performed with isotropic atomic displacement parameters and gave good agreement factors [$R_1(F)$, R_1(0.0001 GPa) = 0.057; R_1(2.28 GPa) = 0.053; R_1(4.61 GPa) = 0.054] (Gatta et al. 2004).

Further details of the room and H*P* data collections, structural refinement strategies, refined atomic positions, thermal displacement parameters and bond distances are reported in Gatta et al. (2004).

Volume and axial compressibility

Lattice parameters of tetragonal edingtonite with pressure are reported in Table 1.

Volume and axial compressibility were calculated using the Birch-Murnaghan equation of state (BM-EoS) (Birch 1947; Angel 2000):

$$P(f) = 3K_0 f(1+2f)^{5/2}\{1 + 3/2(K'-4)f + 3/2[K_0K'' + (K'-4)(K'-3) + 35/9]f^2 + \cdots\},$$

where f is the Eulerian strain ($f = [(V_0/V)^{2/3} - 1] / 2$) . V_0 and V represent the cell volume under ambient and HP conditions, respectively; K_0 is the bulk modulus ($K_0 = -V_0(\partial P/\partial V)_{P=0} = 1/\beta$, where β is the volume compressibility coefficient) and K' and K'' represent its pressure derivatives ($K' = \partial K_0/\partial P$; $K'' = \partial^2 K_0/\partial P^2$).

Table 1 Lattice parameters of tetragonal edingtonite, simulated (*sim*) and experimental (*exp*) ellipticity ratios for [110] and [001] channels, and φ angle values at different pressures. Experimental data from Gatta et al. (2004)

P (GPa)	*a* (Å)	*c* (Å)	*V* (Å^3)	ε[110] sim	ε[110] exp	ε[001] sim	ε[001] exp	φ(°) sim	φ(°) exp
0.0001	9.5909(14)	6.5339(19)	601.03(24)	0.728	0.72[a]	0.363	0.32[a]	15.70	17.15(8)
0.689(8)	9.5602(9)	6.5117(13)	595.15(17)	0.715		0.354		15.98	–
1.080(8)	9.5383(9)	6.5021(13)	591.56(17)	0.705		0.347		16.19	–
1.312(8)	9.5277(33)	6.4988(44)	589.95(56)	0.701		0.345		16.28	–
1.539(8)	9.5117(9)	6.4904(12)	587.21(15)	0.694		0.339		16.44	–
1.998(8)	9.4838(9)	6.4801(13)	582.85(16)	0.682		0.331		16.71	–
2.28(1)	9.4669(24)	6.4765(33)	580.41(41)	0.676	0.66[a]	0.326	0.29[a]	16.87	18.28(7)
2.70(2)	9.4435(9)	6.4651(14)	576.56(17)	0.658		0.321		17.00	–
3.05(1)	9.4239(7)	6.4576(10)	573.51(12)	0.649		0.316		17.19	–
3.45(2)	9.4019(7)	6.4489(10)	570.07(12)	0.639		0.309		17.39	–
4.61(2)	9.3466(6)	6.42705(9)	561.46(10)	0.615		0.293		17.91	–
5.08(3)	9.3279(10)	6.4169(14)	558.34(16)	0.606	0.61[a]	0.288	0.24[a]	18.09	20.03(9)

[a]eds values are about 0.005

The axial compressibilities can be described by an EoS like that used to fit the P–V data, simply by substituting the cube of lattice parameter with the volume (Xia et al. 1998; Angel 2000). The relationship between the linear-K_0 obtained and the linear-axial compressibility (β_j) is:

$$\beta_j = -1/(3K_{0j}) = 1/l_{0j}(\partial l_j/\partial P),$$

where l_{0j} ($j = a, b, c$) is the length of the cell axis under room conditions.

Edingtonite cell-volume data were fitted with a truncated second-order BM-EoS, with the EoS-FIT5.2 program (Angel 2001), using data weighed according to the uncertainties in P and V. The refined parameters are: $V_0 =$ 601.8(2) Å^3, $K_{T0} =$ 57.9(6) GPa ($K' = 4$). A third-order BM-EoS leads to the following parameters: $V_0 =$ 601.6(3) Å^3, $K_{T0} =$ 59(2) GPa, $K' =$ 3.4(8).

As expected for a fibrous zeolite framework, the axial compressibility of edingtonite is strongly anisotropic. The axial bulk moduli calculated with a third-order linearized BM-EoS (Xia et al. 1998; Angel 2000) are: $K_{T0a} =$ 53(3) and $K'_a =$ 2(1) for the a-axis, $K_{T0c} =$ 73(4) and $K'_c =$ 10(2) for the c-axis ($K_{T0a} : K_{T0b} : K_{T0c} =$ 1:1:1.4).

The axial and volume-compression patterns demonstrate that no phase transition is detected within the pressure range investigated (0.0001–5.08 GPa). The HP-deformations induced within the pressure range investigated are completely reversible: the diffraction data during decompression are indistinguishable from the compressive data, and showed a complete restoration of the lattice.

The bulk modulus of edingtonite is slightly higher than the bulk moduli of other fibrous zeolites: for natrolite $K_{T0} =$ 53(1) GPa with $K' = 4$ (before the phase transition at 1.5–2.0 GPa, Lee et al. 2002); for scolecite $K_{T0} =$ 54.6(7) GPa with $K' = 4$ (Comodi et al. 2002).

HP-structural evolution

The HP-structural evolution of edingtonite was studied by comparing the three refinements carried out at 0.0001, 2.28(1) and 4.61(2) GPa. The increasing pressure did not produce relevant variations in the tetrahedral bond distances, since the aluminosilicate framework is characterized by rigid SiO_4/AlO_4 tetrahedra. The bonding inside the tetrahedra is very strong: the bulk modulus of $TO_4(SiO_4)$ is 580(24) GPa (Zhang et al. 1998). Thus, as a first approximation we can consider the primary building unit (the tetrahedron) as infinitely rigid. The polyhedral tilting, which produces inter-tetrahedral angle variations, represents the main deformation mechanism. The first evidence is in the 4 = 1 secondary building unit itself: the angle (T1–O45–T2)° changes from 140.18(8)° at 0.0001 GPa, to 134.34(10)° at 4.61 GPa, whereas in the same pressure range the distance between T2 and T2 decreases from 3.776(5) Å to 3.715(6) Å.

The most relevant structural variation is produced by cooperative rotation (antirotation) of the SBU chains along [001] (Fig. 1). As a consequence, the main effects are observed in the eight-membered ring channels along [001]: the acute angles of the channel (O23–O1–O23)° (Fig. 1) decrease from 79.21(9)° at 0.0001 GPa to 75.75(9)° at 4.61 GPa; on the contrary, in the same pressure range the obtuse angles (O45–O1–O45)° (Fig. 1) increase from 108.74(10) ° to 110.97(12)°. The kinking between the adjacent SBU chains with increasing pressure is well represented by the variation of the angle φ ($\varphi = [180°-(O1–O1–O1)°]/2$; Fig. 1). The φ angle value increases from 17.15(8)° to 20.03(9)° in response to an applied pressure of 4.61 GPa.

The antirotation mechanism induces a change in the shape of the channels. To analyse the variation of ellipticity of the [001] channels with pressure, we calculated the ellipticity ratio (ε) as the ratio between the smaller free diameter (Baerlocher et al. 2001) compared to the larger one: $\varepsilon_{[001]} =$ O1–O1(short)/O1–O1(long) for the eight-ring channel along [001] and $\varepsilon_{[110]} =$ O45–O45(long)/O1–O1 for the eight-ring channel along [110] (Fig. 1). $\varepsilon_{[001]}$ decreases from 0.32 to 0.24 (an increase in ellipticity of about 25%) and $\varepsilon_{[110]}$ from 0.72 to 0.61 (an increase in ellipticity of about 15%), in response to an applied pressure of 4.61 GPa (Table 1). Lee et al. (2002) and Comodi et al. (2002) reported a similar behaviour in the evolution of the channel shapes with pressure for natrolite and scolecite, respectively.

The HP-behaviour of the extra-framework content is extensively treated in Gatta et al. (2004). The main effect is the following: the occupancy of the minority Ba2 site decreased under HP-conditions and, in compensation, the occupancy coefficient for the Ba1 site increased. At 4.61 GPa the Ba2 site is completely empty and only the Ba1 position is occupied. Since the RUM modelling is applied only to the Si/Al framework, we do not examine closely the extra-framework evolution under pressure.

Theoretical approach

Geometric modelling

To examine the framework response to compression in terms of the rigid unit model of silicate frameworks, we make use of a geometric model developed by one of the authors (Wells 2003). In this approach we model the structure in parallel, both as an assemblage of atoms and as a framework of ideal polyhedra. This approach allows us to relax the structure atomistically within a force model based on rigid unit modelling, and to interpret the resulting motions of the atoms in terms of the motions of the polyhedra.

The modelling of compression which we carry out here requires three geometric operations: these are (1) fitting geometrically ideal polyhedra to the real atomic positions, (2) relaxing the atoms towards their geometrically ideal positions, and (3) analyzing the resulting

atomic motions in terms of polyhedral rotations. All of these operations are carried out by a code called GASP (geometric analysis of structural polyhedra). This code is written entirely in Fortran 90 and is available to researchers. The code is described more fully in Wells et al. (2004).

Given the atoms of an SiO_4 unit, we take two Si–O bond directions and use them to establish a basis set of unit vectors. We construct an ideal polyhedron using this basis set and a defined ideal Si–O distance. The resulting ideal polyhedron has its centre at the position of the Si atom; one of its bonds is parallel to one of the Si–O bonds; and the other three ideal bonds will lie close to but not coincident with the remaining three Si–O bonds. We now define a mismatch score M as the sum of the squares of the distances between the real and ideal O sites. This mismatch score we minimize as a function of the parameters of a free rotation of the ideal polyhedron. The result is a least-squares fit of the ideal polyhedron to the real atomic positions.

To relax the atoms, we now apply a spring force acting between each oxygen atom and the ideal O sites defined by the ideal polyhedra. Bridging oxygen atoms will be connected to two ideal sites. For each spring force applied to an oxygen atom an equal and opposite force is applied to the silicon atom at the centre of the ideal polyhedron. We also include spring forces between neighbouring silicon atoms; these constrain the Si–O–Si bridging angle by constraining the Si–Si distance.

Once all the forces on all atoms have been found, a resulting displacement is calculated for each atom, and a new structure generated with the new atomic positions. We can now refit the ideal polyhedra, geometrically, and then continue the relaxation. After several iterations the structure approaches a geometrically ideal condition in which the forces balance.

Essentially, the ideal polyhedra define a multibody interaction, so that every atom relaxes based on the positions of its first- and second-nearest neighbours. Motion of the atoms based on these ideal polyhedra seeks to idealize the O–Si–O and Si–O–Si angles, but these need never be explicitly evaluated. This relaxation process is very rapid for large cells and thus is useful for examining the behaviour of zeolite frameworks.

Once the structure is fully relaxed, we wish to analyze the motions of the atoms in terms of polyhedral rotation. We consider the atoms of the polyhedron before and after the motion. As when fitting ideal polyhedra, we define a mismatch score M as the sum of the squares of the changes of position of the oxygen atoms relative to the silicon atom at the centre of the polyhedron. This mismatch score we then minimize as a function of the parameters of a free rotation of one of the polyhedra.

Rotor operator

We have found it computationally convenient to define rotations using the rotor operator of geometric algebra. This is an object analogous to a quaternion having three independent, orthogonal components: B_x, B_y, B_z. The rotor with parameters (B_x, B_y, B_z), where $|\mathbf{B}| = (B_x^2 + B_y^2 + B_z^2)^{0.5}$, represents a rotation by an angle $\theta = 2\arcsin(|\mathbf{B}|/2)$ about an axis b_x,b_y,b_z, where b is the unit vector such that

$$b_x^2 + b_y^2 + b_z^2 = 1,$$

$$b_x : b_y : b_z = B_x : B_y : B_z.$$

So, to first order, B_x represents the rotation, in radians, about the x axis, and so on. We report the rotations of the polyhedra during compression by giving the values of B_x, B_y, B_z.

Simulation of compression mechanism

The simplest proposed compression mechanism is based on the anti-rotation of adjacent SBU chains. We model compression using a large supercell ($2 \times 2 \times 2$) of the original structure, containing a total of 16 SBUs (i.e. 80 polyhedra, 240 atoms) without any symmetry-imposed restraints. Since the geometric modelling process is very local (each polyhedron communicates only with its immediate neighbours), it is not demanding to study even these large cells. We begin by maintaining all atoms at the fractional coordinates of the zero-pressure structure; we simulate compression by imposing the cell parameters obtained experimentally at a given pressure. We then run multiple iterations of the geometric relaxation described above, so that the structure relaxes towards the ideal polyhedral shapes and bridging angles for a silica framework. All structures were relaxed for 40 iterations of the relaxation routines, which was more than sufficient for the changes in atomic positions to become negligible. We thus obtain the rigid-unit response of the structure to the compression.

We can analyze the rotational motions of the polyhedra by comparing the polyhedra in a compressed structure to those in the zero-pressure structure using the least-squares approach described above. For each polyhedron we obtain a rotor describing its rotation relative to the zero-pressure structure. We can track the components of the rotor as a function of pressure and thus describe the framework response to compression. In our results we use this analysis to describe the response of the SBU to compression.

We wish to extract from our simulation a measure directly comparable with experiment. Our chosen measure is the channel ellipticity of the channels along the [001] and [110] directions. As discussed above, this is the ratio of the long and short free diameters of the channels: that is, the distance between the oxygen sites, less twice the radius of an oxygen atom, which radius we take to be 1.35 Å, according to Baerlocher et al. (2001).

Since in this simulation we are not restricted to using the experimentally determined cell parameters, we can also simulate uniaxial compression along the z-axis, and

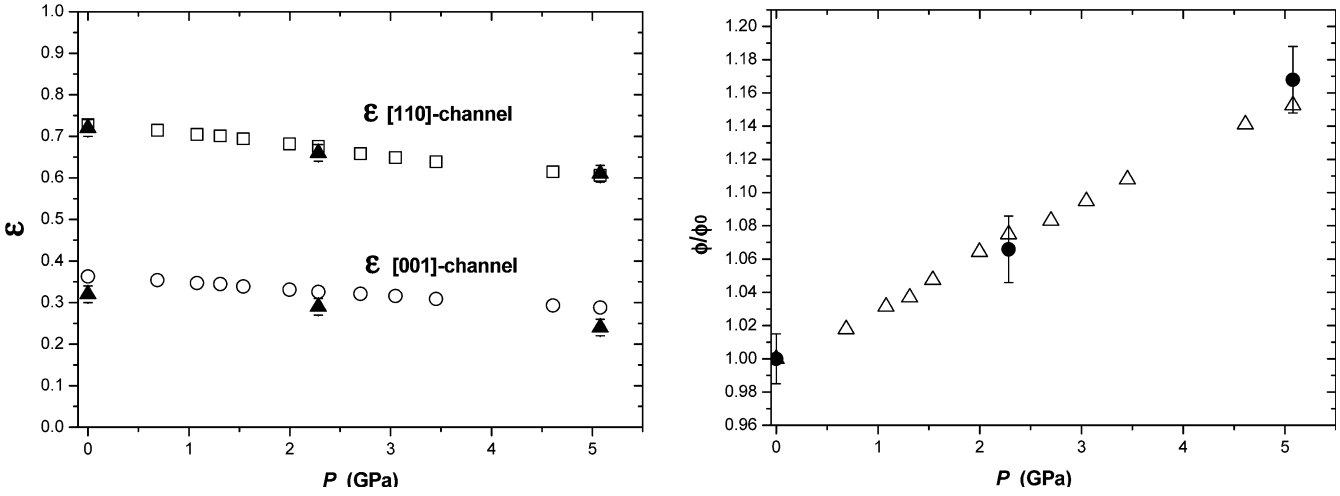

Fig. 2 Experimental (*full symbols*) and simulated (*open symbols*) values of the channel ellipticity ratios and of the φ angle (normalized to the ambient value) according to Table 1. For the experimental data, 3σ *error bars* are shown

compression in the *xy*-plane only. By simulating these non-hydrostatic compression regimes, which are difficult to access experimentally, we can shed more light on the details of the compression mechanism.

Tables with the atomic positions of the simulated crystal structure under hydrostatic and non-hydrostatic conditions are deposited and available in the form of CIF files as supplementary electronic materials.

Results

Channel ellipticities

The channel ellipticities for the [001] and [110] channels as a function of pressure are given in Table 1. For both channels the ellipticity ratio decreases with pressure (Fig. 2), in accordance with the experimental data. The simulation of the [110] channel ellipticity reproduces the experimental data very well. The [001] channel ellipticity ratio is consistently higher than the experimental value by approximately 0.04 [at zero pressure, $\varepsilon_{[001]} = 0.363$ (sim), 0.32 (exp); at 5.08 GPa, $\varepsilon_{[001]} = 0.288$ (sim), 0.24 (exp)]. We attribute this difference to the approximations made in the geometric simulation (neglect of electrostatic interactions and channel contents). The differences between the simulated and experimental results are throughout less than $6\sigma(\varepsilon_{exp})$. The variation of the ellipticity ratio with pressure agrees with the experimental data, as shown in Fig. 2.

The ellipticity increase with pressure is an effect of the main deformation mechanism, a cooperative rotation of the SBU (Fig. 1), in accordance with the experimental data. This antirotation mechanism can be quantified by the φ angle value, which describes the relative rotation of each SBU with respect to the adjacent one. Here, too, the variation of the φ angle with pressure is in good agreement with the experimental results (Table 1; Fig. 2).

Polyhedral rotations within an SBU

Although the simplest picture of the compression mechanism is the antirotation of adjacent SBUs, in fact we find that the behaviour is more complex than this. Each SBU contains one T1 site and four T2 sites. We find that the T1 site rotates only about the *z*-axis (Table 2). The T2 sites, however, display general rotations in which the *z* component of the rotor is not dominant but rather is the smallest component of the rotor (Table 2). We plot the behaviour of the rotor components for selected T1

Table 2 Simulated T1 and T2 polyhedral rotor components with respect to *x*, *y* and *z*-axis and net rotation under hydrostatic conditions

P (GPa)	T1-*X* (rad)[a]	T1-*Y* (rad)	T1-*Z* (rad)	T1-net (rad)	T2-*X* (rad)	T2-*Y* (rad)	T2-*Z* (rad)	T2-net (rad)
0.689	0.0000	0.0000	0.0179	0.0179	0.0088	0.0042	0.0028	0.0101
1.080	−0.0001	0.0001	0.0307	0.0307	0.0147	0.0065	0.0048	0.0168
1.312	0.0000	0.0000	0.0350	0.0350	0.0171	0.0074	0.0059	0.0195
1.539	0.0000	0.0001	0.0449	0.0449	0.0214	0.0092	0.0075	0.0245
1.998	0.0000	0.0000	0.0593	0.0593	0.0281	0.0117	0.0104	0.0322
2.28	−0.0001	0.0002	0.0672	0.0672	0.0317	0.0128	0.0124	0.0363
2.70	−0.0003	0.0002	0.0902	0.0902	0.0447	0.0169	0.0119	0.0493
3.05	0.0006	0.0006	0.1013	0.1013	0.0505	0.0186	0.0134	0.0555
3.45	0.0001	−0.0003	0.1137	0.1137	0.0557	0.0206	0.0157	0.0614
4.61	0.0003	0.0001	0.1454	0.1454	0.0714	0.0258	0.0205	0.0787
5.08	0.0007	−0.0002	0.1576	0.1576	0.0771	0.0276	0.0219	0.0848

[a] 1 rad ≈ 57.295780 deg

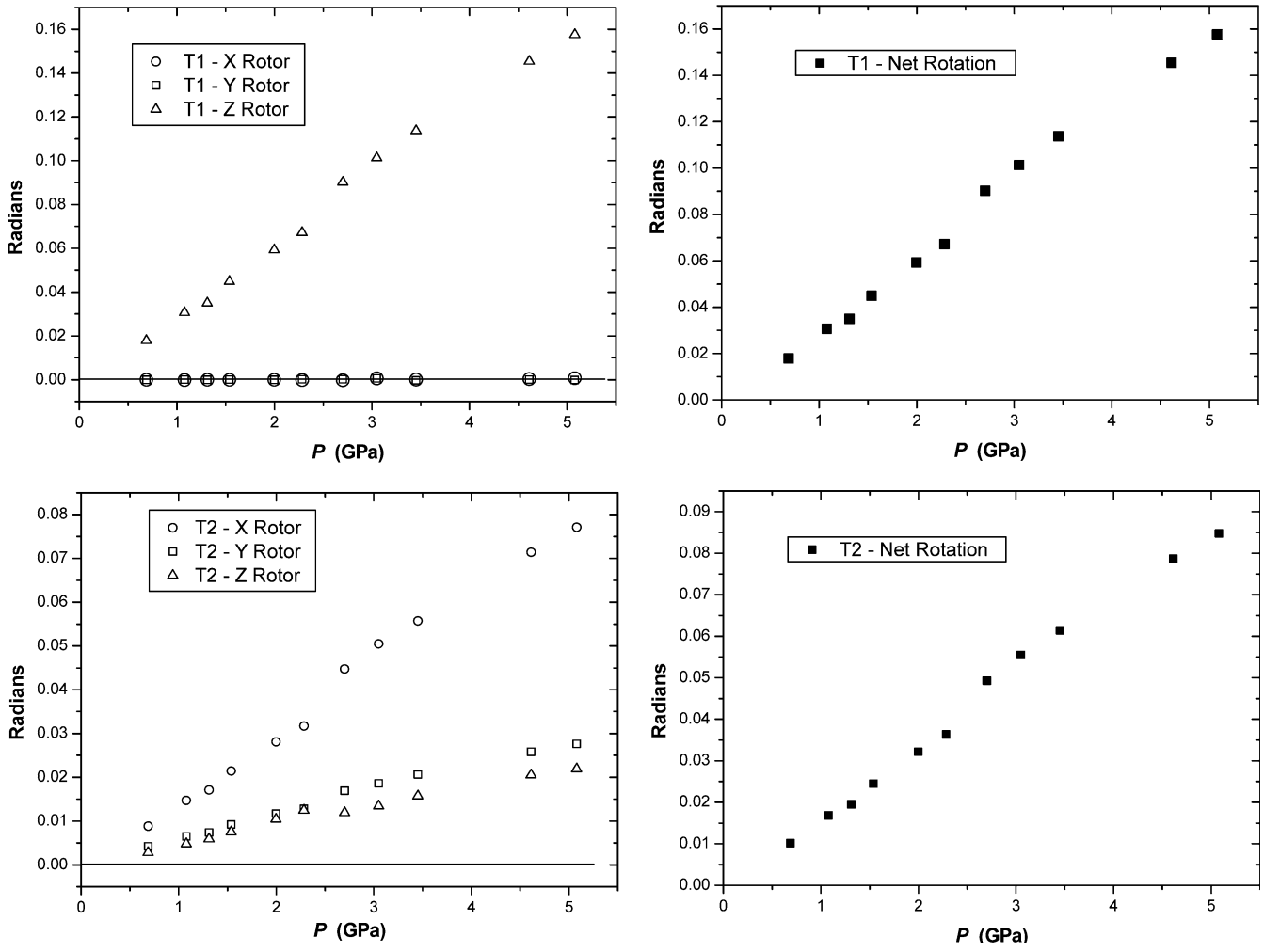

Fig. 3 Simulated polyhedral rotor components with respect to *x*, *y* and *z*-axis and net rotation under hydrostatic conditions

Table 3 Simulated polyhedral rotation and channel ellipticity under non-hydrostatic conditions: uniaxial compression along *z*, and in the *xy*-plane

Compression along *z*										
Shortening of *c* (%)	T1-*X* (rad)[a]	T1-*Y* (rad)	T1-*Z* (rad)	T1-net (rad)	T2-*X* (rad)	T2-*Y* (rad)	T2-*Z* (rad)	T2-net (rad)	ε[110]	ε [001]
0	–	–	–	–	–	–	–	–	0.728	0.363
1	0.0000	–0.0001	0.0224	0.0224	0.0133	0.0086	0.003	0.0161	0.725	0.362
2	0.0000	–0.0001	0.0457	0.0457	0.0275	0.0172	0.0065	0.0331	0.722	0.363
3	0.0002	–0.0001	0.0704	0.0704	0.0429	0.026	0.0104	0.0512	0.717	0.363
Compression on the xy-plane										
Shortening of *a* and *b* (%)	T1-*X* (rad)	T1-*Y* (rad)	T1-*Z* (rad)	T1-net (rad)	T2-*X* (rad)	T2-*Y* (rad)	T2-*Z* (rad)	T2-net (rad)	ε[110]	ε[001]
0	–	–	–	–	–	–	–	–	0.728	0.363
1	0.0000	0.0000	0.0370	0.0370	0.0156	0.0046	0.0111	0.0197	0.689	0.335
2	–0.0001	0.0001	0.0750	0.0750	0.0316	0.0086	0.0229	0.0399	0.651	0.307
3	–0.0001	0.0001	0.1150	0.1150	0.0485	0.0124	0.0347	0.0609	0.611	0.278

[a]1 rad ≈ 57.295780 deg

and T2 sites in Fig. 3, where we have chosen sites for which all the rotor components are positive.

The net rotation of the T2 site is approximately half that of the T1 site (Fig. 3). The response of the SBU to compression, therefore, is not simply a bodily rotation about the *z*-axis, but rather a rotation of the T1 site about the *z*-axis, accompanied by rotations of the T2 sites about axes lying closer to the *xy*-plane than to the

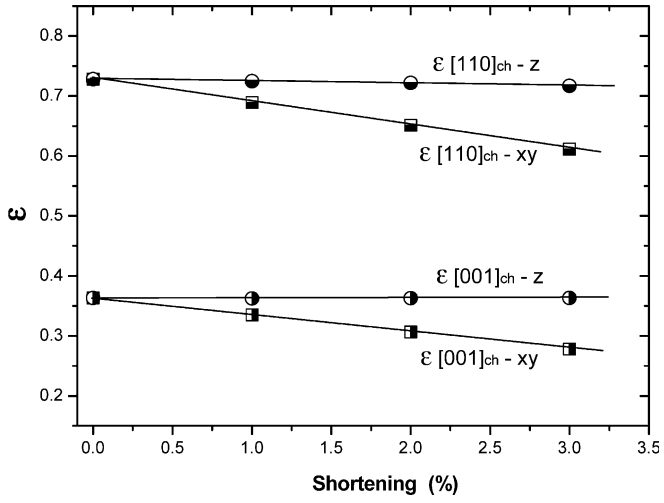

Fig. 4 Simulated channel ellipticity evolution under non-hydrostatic compression: uniaxial compression along *z*, and in the *xy*-plane. The compression (on the horizontal coordinate) is given as shortening (%) along the *z* or the *x*–*y*-axis

Fig. 5 Simulated polyhedral rotor components with respect to *x*-, *y*- and *z*-axis and net rotation under non-hydrostatic conditions: uniaxial compression along *z*, and in the *xy*-plane

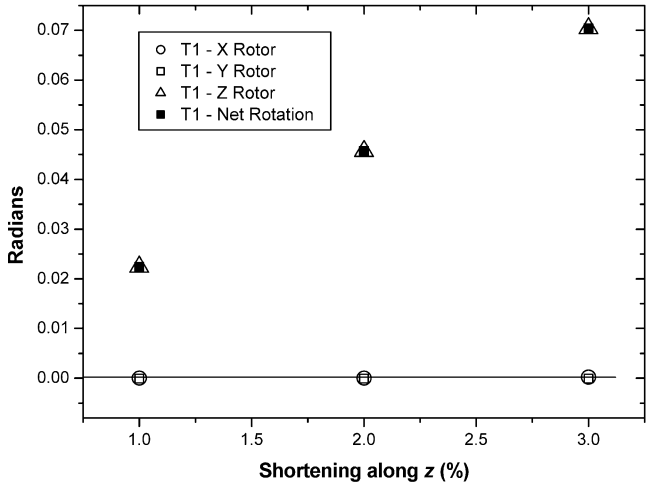

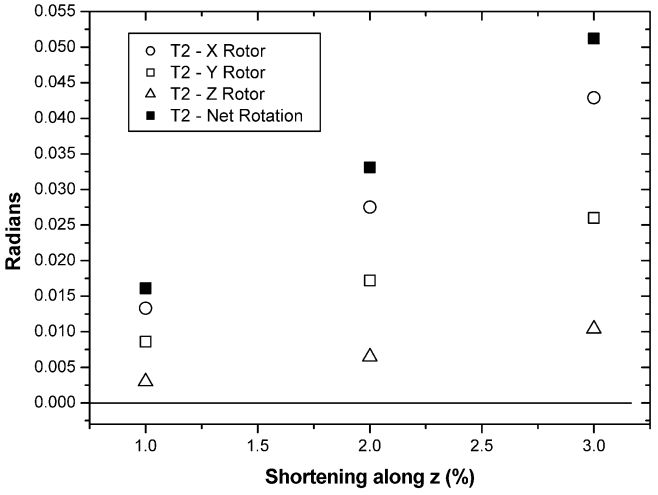

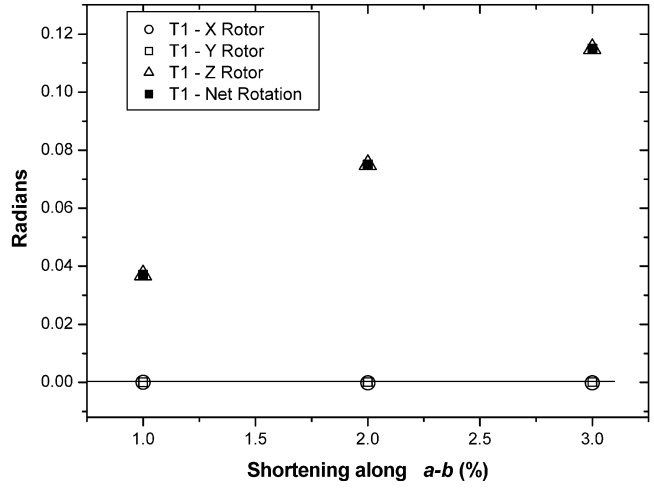

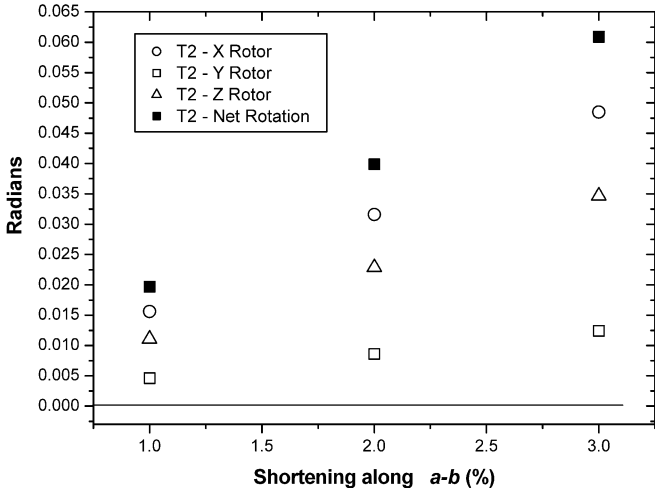

z-axis. These, coupled with displacements of the T2 sites in the *xy*-plane, make up the response of the SBU.

Simulation of uniaxial compression

To investigate the compression mechanism in more detail, we have also simulated uniaxial compression along the *z*-axis and compression in the *xy*-plane. In these cases, rather than impose the cell parameters obtained experimentally during compression, we simply reduce one of the cell parameters (*a* or *c*) by 1, 2 or 3% and then relax the structure geometrically. The simulated values of the channel ellipticities and rotor components for the T1 and T2 tetrahedra under non-hydrostatic compression are in Table 3.

The behaviour of the channel ellipticites with pressure is shown in Fig. 4. The results are a little surprising. The response of the channels to compression in the *xy*-plane (reduction of the *a* and *b* parameter only) appears very similar to the response to hydrostatic compression, with an increase in ellipticity for both the [001] and [110] channels. The response to compression along the *z*-axis, however, is almost non-existent: the ellipticity of both channels remains constant. Although we might expect

the ellipticity of the [001] channels to be unaffected by compression along the *z*-axis, it seems odd that the [110] channels should also retain their shape.

The behaviour of the rotor components for the T1 and T2 sites is shown in Fig. 5. During compression along the *z*-axis, the T1 sites antirotate around the *z*-axis, causing the oxygen atoms defining the edges of the [110] channels to move towards each other in the *xy*-plane. Thus, rather than contracting along the *z*-axis (with a consequent decrease in ellipticity), the [110] channels contract isotropically. On compression in the *xy*-plane the T1 sites rotate about the *z*-axis, as during hydrostatic compression. The T2 sites display a smaller magnitude of rotation than the T1 sites, and the *z* component of the rotor is the second-largest component. On compression along the *z*-axis, the T1 sites still rotate about the *z*-axis, but with a smaller rotation angle than during *xy* compression. The rotation of the T2 sites is similar in magnitude to that during *xy* compression, but the *z* component of the rotor is now the smallest component.

We conclude, therefore, that the change in channel ellipticity during hydrostatic compression is, in fact, due to the compression in the *xy*-plane, as the compression along the *z*-axis leads to an isotropic shrinkage of the channels rather than to a change in ellipticity.

A movie, available as electronic supplementary material, made by a sequence of crystal structure pictures under oriented compression (along *z* and on the *xy*-plane), reveals the mechanisms at work.

Comparison of experimental and theoretical findings

We find from the study of compression under hydrostatic conditions that the RUM simulation results are in good agreement with the experimental findings.

The main structural deformation mechanism observed by experiment is the cooperative rotation of the SBU along [001]. This mechanism is perfectly reproduced by the simulated evolution of the crystal structure under pressure.

The geometrical modelling shows that the response of the SBU to compression is not a simple bodily rotation about the *z*-axis: a rotation of the T1 site about the *z*-axis is accompanied by rotations of the T2 sites about axes lying closer to the *xy*-plane; these two mechanisms change the configuration of the SBU itself. This result is in agreement with Gatta et al. (2004), who describe the SBU as a non-infinitely rigid unit, with a bulk modulus value of about 100 GPa.

The experimental response to pressure of both the [001] and [110] channel ellipticities is well described by the geometric simulation. The ellipticity of the [001] channels is consistently slightly underestimated by the geometric simulation ($\varepsilon_{[001]}$ in the simulation is higher than the experimental finding by approximately 0.04 at all pressures). The principle cause of the discrepancy is probably that the geometric simulation does not include either electrostatic interactions or channel contents, being purely a geometric representation of the tetrahedral framework. The absence of these interactions will cause the polyhedra to be too close to geometric perfection; in practice, for example, oxygen atoms would interact with the barium cations in the channels, with a consequent polarization-distortion of the tetrahedra. However, the discrepancy is sufficiently small that we can say that the simulation provides a good description of the framework behaviour during compression.

The simulation of uniaxial compression allows us to investigate a regime which we cannot access by experiment. This leads us to the unexpected conclusion that compression of the structure along the *z*-axis leads to an isotropic contraction of the channels, and that the change in channel ellipticity with pressure is due to the compression in the *xy*-plane.

Conclusion

This comparative study on the high pressure behaviour of a fibrous zeolite shows the reliability of the RUM modelling in open-framework silicates with a complicated crystal structure, characterized by large channels and a framework that is very flexible but has rigid units. H*P* experimental and simulated data agree that the flexibility possessed by this family of framework microporous silicates is related to a few specific deformation modes, due to stiff tetrahedra (primary building unit) and flexible oxygen hinges.

For the edingtonite crystal structure, the $4 = 1$ secondary building unit appears not to be infinitely rigid: experimental and simulated structural H*P*-behaviours show that the fibrous zeolite SBU slightly changes its original configuration in response to the applied pressure, contributing to the lattice compressibility. The local and global *P*-induced deformation mechanisms of the Si/Al framework observed by experiment (channel ellipticity, SBU rotation) are well reproduced by RUM modelling.

Acknowledgements Wilson Crichton (ESRF-Grenoble) and an anonymous referee are gratefully acknowledged for their useful comments.

References

Allan DR, Miletich R, Angel RJ (1996) A diamond-anvil cell for single-crystal X-ray diffraction studies to pressures in excess of 10 GPa. Rev Sci Instrum 67: 840–842

Angel RJ (2000) Equation of state. In Hazen RM, Downs RT (eds) High-temperature and high-pressure crystal chemistry. Reviews in Mineralogy and Geochemistry, vol 41, Mineralogical Society of America and Geochemical Society, Washington, DC, pp 35–59

Angel RJ (2001) EOS-FIT V6.0. Computer program. Crystallography Laboratory, Dept. Geological Sciences, Virginia Tech, Blacksburg, USA

Angel RJ (2002) ABSORB V5.2. Computer program. Crystallography Laboratory, Dept. Geological Sciences, Virginia Tech, Blacksburg, USA

Angel RJ (2003a) Automated profile analysis for single-crystal diffraction data. J Appl Crystallogr 36: 295–300

Angel RJ (2003b) Win-IntegrStp V3.4. Computer program. Crystallography Laboratory, Dept. Geological Sciences, Virginia Tech, Blacksburg, USA

Angel RJ, Allan DR, Miletich R, Finger LW (1997) The use of quartz as an internal pressure standard in high pressure crystallography. J Appl Crystallogr 30: 461–466

Angel RJ, Downs RT, Finger LW (2000) High-temperature—high-pressure diffractometry. In: Hazen RM, Downs RT (eds) High-temperature and high-pressure crystal chemistry. Reviews in Mineralogy and Geochemistry, vol 41, Mineralogical Society of America and Geochemical Society, Washington, DC, pp 559–596

Armbruster T, Gunter ME (2001) Crystal structures of natural zeolites. In: Bish DL, Ming DW (eds) Natural zeolites: occurrence, properties, application. Reviews in Mineralogy and Geochemistry, vol 45, Mineralogical Society of America and Geochemical Society, Washington, DC, pp 1–57

Baerlocher Ch, Meier WM, Olson DH (2001) Atlas of zeolite framework types, 5th edn. Elsevier, Amsterdam, 302 pp

Ballone P, Quartieri S, Sani A, Vezzalini G (2002) High pressure deformation mechanism in scolecite: a combined computational-experimental study. Am Mineral 87: 1194–1206

Belitsky IA, Gabuda SP, Joswig W, Fuess H (1986) Study of the structure and dynamics of water in the zeolite edingtonite at low temperature by neutron diffraction and NMR-spectroscopy. N Jb Miner Mh 1986: 541–551

Belitsky IA, Fursenko BA, Gabuda SP, Kholdeev OV, Seryotkin YV (1992) Structural transformation in natrolite and edingtonite. Phys Chem Miner 18: 497–505

Birch F (1947) Finite elastic strain of cubic crystal. Phys Rev 71: 809–824

Bish DL, Vaniman DT, Chipera SJ, Carey JW (2003) The distribution of zeolites and their effects on the performance of a nuclear waste repository at Yucca Mountain, Nevada, USA. Am Mineral 88: 1889–1902

Burnham CW (1966) Computation of absorption corrections and the significance of end effects. Am Mineral 51: 59–167

Comodi P, Gatta GD, Zanazzi PF (2002) High pressure behaviour of scolecite. Eur J Mineral 14: 567–574

Dove MT, Heine V, Hammonds KD (1995) Rigid unit modes in framework silicates. Min Mag 59: 629–639

Dove MT, Gambhir M, Hammonds KD, Heine V, Pryde AKA (1996) Distortions of framework structures. Phase Trans 58: 121–143

Forman RA, Piermarini G J, Barnett JD, Block S (1972) Pressure measurement made by utilisation of ruby sharp-line luminescence. Science 176: 284–286

Galli E (1976) Crystal structure refinement of edingtonite. Acta Crystallogr (B) 32: 1623–1627

Gatta GD, Boffa Ballaran T (2004) New insight into the crystal structure of orthorhombic edingtonite. Min Mag 68: 167–175

Gatta GD, Comodi P, Zanazzi PF (2003) New insights on high pressure behaviour of microporous materials from X-ray single-crystal data. Micr Mesop Mat 61: 105–115

Gatta GD, Boffa Ballaran T, Comodi P, Zanazzi PF (2004) Isothermal equation of state and compressional behaviour of tetragonal edingtonite. Am Mineral 89: 633–639

Gillet P, Malézieux JM, Itié JP (1996) Phase changes and amorphization of zeolites at high pressure: the case of scolecite and mesolite. Am Mineral 81: 651–657

Gottardi G, Galli E (1985) Natural Zeolites, Springer-Verlag, Berlin, D, 409 pp

Goryainov SV, Kursonov AV, Miroshnichenko YuM, Smirnov MB, Kabanov IS (2003) Low-temperature anomalies of infrared band intensities and high pressure behaviour of edingtonite. Micr Mesop Mat 61: 283–289

Hammonds KD, Deng H, Heine V, Dove MT (1997) How floppy modes give rise to adsorption sites in zeolites. Phys Rev Lett 78: 3701–3704

Kallo D (2001) Applications of natural zeolites in water and wastewater treatment. In Bish DL, Ming DW (eds) Natural zeolites: occurrence, properties, application. Reviews in Mineralogy and Geochemistry, vol. 45, Mineralogical Society of America and Geochemical Society, Washington, DC, pp 519–550

King HE, Finger LW (1979) Diffracted beam crystal centering and its application to high pressure crystallography. J Appl Crystallogr 12: 374–378

Kvick A, Smith JV (1983) A neutron diffraction study of the zeolite edingtonite. J Chem Phys 79: 2356–2362

Lee Y, Vogt T, Hriljac JA, Parise JB, Artioli G (2002) Pressure-induced volume expansion of zeolites in the natrolite family. J Am Chem Soc 124: 5466–5475

Lee Y, Hriljac JA, Studer A, Vogt T (2004) Anisotropic compression of edingtonite and thomsonite to 6 GPa at room temperature. Phys Chem Miner 31: 22–27

Mao HK, Xu J, Bell PM (1986) Calibration of the ruby pressure gauge to 800 kbar under quasi-hydrostatic conditions. J Geophys Res 91: 4673–4676

Mazzi F, Galli E, Gottardi G (1984) Crystal structure refinement of two tetragonal edingtonites. N Jb Miner Mh 1984: 373–382

Ming DW, Allen ER (2001) Use of natural zeolites in agronomy, horticulture, and environmental soil remediation. In Bish DL, Ming DW (eds) Natural zeolites: occurrence, properties, application. Reviews in Mineralogy and Geochemistry, vol 45, Mineralogical Society of America and Geochemical Society, Washington, DC, pp 619–654

Sheldrick GM (1996) SADABS. Program for empirical absorption correction of area detector data. Institut für Anorg. Chemie, University of Göttingen, Germany

Sheldrick GM (1997) SHELX-97. Programs for crystal structure determination and refinement. Institut für Anorg. Chemie, University of Göttingen, Germany

Ståhl K, Hanson JC (1998) An in situ study of the edingtonite dehydration process from X-ray synchrotron powder diffraction. Eur J Mineral 10: 221–228

Taylor WH, Jackson R (1933) The structure of edingtonite. Z Kristallogr 86: 53–64

Tchernev DI (2001) Natural zeolites in solar energy, heating, cooling, and energy storage. In Bish DL, Ming DW (eds) Natural zeolites: occurrence, properties, application. Reviews in Mineralogy and Geochemistry, vol. 45, Mineralogical Society of America and Geochemical Society, Washington, DC, pp 589–618

Wells SA, Dove MT, Tucker M (2004) Reverse Monte Carlo with geometric analysis- RMC + GA. J Appl Crystallogr (in press).

Wells SA (2003) Real-space rigid unit analysis of framework structures using geometric algebra, PhD Thesis, Department of Earth Sciences, University of Cambridge, UK

Wells SA, Dove MT, Tucker M (2002a) Finding best-fit polyhedral rotations with geometric algebra. J Phys: Condens Matter 14: 4567–4584

Wells SA, Dove MT, Tucker M, Trachenko K (2002b) Real-space rigid-unit-mode analysis of dynamic disorder in quartz, cristobalite and amorphous silica. J Phys: Condens Matter 14: 4645–4657

Xia X, Weidner DJ, Zhao H (1998) Equation of state of brucite: single-crystal Brillouin spectroscopy study and polycrystalline pressure-volume-temperature measurement. Am Mineral 83: 68–74

Zhang L, Ahsbahs H, Kutoglu A (1998) Hydrostatic compression and crystal structure of pyrope to 33 GPa. Phys Chem Miner 19: 507–509

Zheng N, Bu X, Feng P (2003) Synthetic design of crystalline inorganic chalcogenides exhibiting fast-ion conductivity. Nature 426: 428–432